LAGRANGIAN VORTEX LOOPS METHOD FOR HYDRODYNAMIC LOADS COMPUTATION IN 3D INCOMPRESSIBLE FLOWS

SERGEY A. DERGACHEV[1], ILIA K. MARCHEVSKY[1,2] AND GEORGY A. SHCHEGLOV[1,2]

[1] Bauman Moscow State Technical University
2-nd Baumanskaya st., 5, 105005 Moscow, Russia

[2] Ivannikov Institute for Sysyem Programming of the Russian Academy of Sciences
Alexander Solzhenitsyn st., 25, 109004 Moscow, Russia

iliamarchevsky@mail.ru,   shcheglov_ga@bmstu.ru

Key words: Vortex Method, 3D Flow, No-slip Boundary Condition, Boundary Integral Equation, Double Layer Potential, Vortex Loop

Abstract. A new approach is developed for incompressible 3D flow simulation around bodies by Lagrangian vortex method. Closed vortex loops are considered as vortex elements, which are generated on all the body surface and provide the satisfaction of the no-slip boundary condition. The procedure of double layer potential density reconstruction is considered, which consists of two steps. Firstly, the integral equation with respect to vortex sheet intensity is solved, which expresses the equality between the tangential components of flow velocity limit value and the body surface velocity. It is solved by using Galerkin approach. Secondly, the least-squares procedure is implemented, which permits to find nodal values of the double layer potential density. It is shown that the developed algorithm makes it possible to improve significantly the quality of solution for the bodies with very complicated geometry and low-quality surface meshes. The combination of this approach with vortex wake modelling with vortex loops, permits to simulate unsteady flows with higher resolution with acceptable numerical complexity. It can be useful for CFD applications and visual effects reproducing in computer graphics.

1 INTRODUCTION

Vortex methods are well-known tool for unsteady incompressible flows simulation and coupled FSI-problems solution in engineering applications [1, 2]. These methods are also useful in computer graphics in visual effects simulation [3]. One of the key problems in vortex methods is connected to boundary condition satisfaction with high accuracy.

There are number of known models of vortex elements for flow simulation around 3D bodies: closed vortex framework, vortex filament, vorton, vortex dipole, vortex fragmenton, etc. Each of them has some advantages and restrictions. In "classical" vortex

element methods, for example, in the discrete vortex method [4], vorticity is concentrated in vortex framework segments and it is absent outside them in the flow. However, this method requires number of empirical models to determine the location of the vortex sheet separation lines. In case of vortex methods with vortex particles (vortons, vortex blobs, etc.) flow separation zones are formed "naturally" due to vorticity flux approach – vortex elements are generated on the whole body surface and these elements self-organization in the flow [5, 6]. The main part of the vorticity is concentrated in neighbourhood of the vortex elements themselves, however, there is distributed non-zero "additional" vorticity in the flow domain, according to the Helmholtz theorems. Its intensity vanishes far from vortex elements. This additional vorticity may cause significant errors, both at computing aerodynamic loads acting the body, and the boundary condition satisfaction, because the "virtual" velocity field inside the body is not vorticity-free.

Some interesting approach has been proposed in [3] for 3D smoke dynamics simulation, which implies vorticity flux simulation through vortex loops generation of equal circulation on the body surface on the basis of the double layer potential density, which, in turn, provides the boundary condition satisfaction.

The aim of this paper is new numerical approach development in order to improve the existing numerical schemes of vortex methods.

2   INTEGRAL EQUATIONS ARISING IN VORTEX METHODS

The problem of 3D incompressible flow simulation around an immovable body is considered. The governing equations are the Navier – Stokes equations with no-slip boundary conditions on the body surface K and perturbation decay conditions.

It is well-known from physical point of view, that in order to take into account the presence of the body in the flow, it is possible to replace it with the vortex sheet of unknown intensity $.\boldsymbol{\gamma}(\boldsymbol{r})$, placed on the body surface, $.\boldsymbol{r} \in K$, which generates the velocity field $\boldsymbol{V}_\gamma(\boldsymbol{r})$. Then the summary velocity field is the superposition of the incident flow velocity $\boldsymbol{V}_\infty$, velocity field, generated by vorticity inside the flow domain $\boldsymbol{V}_\Omega(\boldsymbol{r})$, and the introduced field $\boldsymbol{V}_\gamma(\boldsymbol{r})$:

$$\boldsymbol{V}(\boldsymbol{r}) = \boldsymbol{V}_\infty + \boldsymbol{V}_\Omega(\boldsymbol{r}) + \boldsymbol{V}_\gamma(\boldsymbol{r}).$$

From mathematical point of view, the velocity $\boldsymbol{V}_\gamma$ potential can be expressed through unknown double layer potential density $g(\boldsymbol{r})$ [4]:

$$\Phi(\boldsymbol{r}) = \frac{1}{4\pi} \oint_K g(\boldsymbol{\xi}) \frac{\partial}{\partial \boldsymbol{n}(\boldsymbol{\xi})} \frac{1}{|\boldsymbol{r} - \boldsymbol{\xi}|} dS_\xi.$$

Note, that the velocity field, which corresponds to this potential

$$\boldsymbol{V}_\gamma(\boldsymbol{r}) = \nabla\Phi(\boldsymbol{r}) = \frac{1}{4\pi} \oint_K g(\boldsymbol{\xi}) \frac{\partial}{\partial \boldsymbol{n}(\boldsymbol{r})} \frac{\partial}{\partial \boldsymbol{n}(\boldsymbol{\xi})} \frac{1}{|\boldsymbol{r} - \boldsymbol{\xi}|} dS_\xi, \tag{1}$$

also can be written down in the following form [4]:

$$\boldsymbol{V}_\gamma(\boldsymbol{r}) = \nabla\Phi(\boldsymbol{r}) = \frac{1}{4\pi} \oint_K \frac{\boldsymbol{\gamma}(\boldsymbol{\xi}) \times (\boldsymbol{r} - \boldsymbol{\xi})}{|\boldsymbol{r} - \boldsymbol{\xi}|^3} dS_\xi, \tag{2}$$

where vector $\gamma(\boldsymbol{r}) = -\operatorname{Grad} g(\boldsymbol{r}) \times \boldsymbol{n}(\boldsymbol{r})$; Grad is surface gradient operator. One can notice, that the expression (2) coincides with the Biot – Savart law for incompressible flows. So the potential $g(\boldsymbol{r})$ is closely connected with vortex sheet intensity $\gamma(\boldsymbol{r})$. The velocity $\boldsymbol{V}(\boldsymbol{r})$ is discontinuous at the body surface; its limit value is

$$\boldsymbol{V}_-(\boldsymbol{r}) = \boldsymbol{V}(\boldsymbol{r}) - \frac{\operatorname{Grad} g(\boldsymbol{r})}{2} = \boldsymbol{V}(\boldsymbol{r}) - \frac{\gamma(\boldsymbol{r}) \times \boldsymbol{n}(\boldsymbol{r})}{2}, \quad \boldsymbol{r} \in K.$$

Taking into account the no-slip boundary condition in the form $\boldsymbol{V}_- = \boldsymbol{0}$ at the body surface, we obtain form (1) and (2) two forms of the integral equation:

$$\frac{1}{4\pi} \oint_K g(\boldsymbol{\xi}) \frac{\partial}{\partial \boldsymbol{n}(\boldsymbol{r})} \frac{\partial}{\partial \boldsymbol{n}(\boldsymbol{\xi})} \frac{1}{|\boldsymbol{r} - \boldsymbol{\xi}|} dS_\xi - \frac{\operatorname{Grad} g(\boldsymbol{r})}{2} = -(\boldsymbol{V}_\infty + \boldsymbol{V}_\Omega(\boldsymbol{r})), \quad \boldsymbol{r} \in K, \quad (3)$$

or

$$\frac{1}{4\pi} \oint_K \frac{\gamma(\boldsymbol{\xi}) \times (\boldsymbol{r} - \boldsymbol{\xi})}{|\boldsymbol{r} - \boldsymbol{\xi}|^3} dS_\xi - \frac{\gamma(\boldsymbol{r}) \times \boldsymbol{n}(\boldsymbol{r})}{2} = -(\boldsymbol{V}_\infty + \boldsymbol{V}_\Omega(\boldsymbol{r})), \quad \boldsymbol{r} \in K. \quad (4)$$

It is proven in [7], that in order to satisfy these equations, it is enough to satisfy them, being projected either on surface normal unit vector or on tangential plane.

3 DOUBLE LAYER POTENTIAL DENSITY DIRECT RECONSTRUCTION

The most common approach to solve of the problem is the equation (3) projection on normal unit vector, that leads to the hypersingular integral equation with respect to the double layer potential [8]. Its solution is normally found as piecewise-constant double layer density on surface mesh, which consists of polygonal panels. The efficient numerical formulae for the Hadamard principal values calculation of hypersingular integrals are suggested by I. K. Lifanov [4].

Note, that the i-th polygonal panel with double layer potential density $g_i = \operatorname{const}$ put exactly the same contribution $\boldsymbol{V}_\gamma^{(i)}$ to the velocity field as closed vortex filament, placed on the panel circumfery, with circulation $\Gamma_i = g_i$. So the vorticity on the body surface automatically becomes represented as closed vortex lines, that corresponds to the Helmholtz fundamental theorems [9].

Numerical experiments show that such approach works satisfactory for flows simulation around smooth bodies of rather simple shape, when the surface mesh is close to uniform. However, even in this case the directions of vortex line on the body surface is determined by the mesh, and can differ significantly from true vorticity surface distribution. This can lead to significant error in velocity field reconstruction in neighborhood of the body surface, especially in the case of unsteady flow simulation around the body with vorticity generation on the surface (vorticity flux model) [1].

The mentioned problems can be overcomed by closed vortex filaments (vortex loops) reconstruction. Positions and circulations of vortex loops can be found according to the following algorithm [3, 10]:

1. the double layer potential density values are calculated at the surface triangular mesh vertices; if the surface mesh consists of polygonal cells, they should be split into triangular sub-panels, maybe by introducing additional nodes;

2. the double layer potential surface distribution is reconstructed by FEM-type interpolation using 1-st order shape functions;

3. vortex loops are generated along the level lines of this potential; vortex loops circulations are determined by the difference between potential density values at the neighboring level lines.

Such approach works perfect, for example, in computer graphics applications [3], where it is enough to provide only qualitative results and high accuracy is not required. Its usage for flow simulation and hydrodynamic forces calculation is restricted, again, with rather simple body geometries and uniform meshes [10].

4   VORTEX SHEET INTENSITY RECONSTRUCTION

The other way to the boundary condition satisfaction is developed in [7, 11] and it supposes the equation (4) projection on the tangential plane. It leads to the 2-nd kind equation

$$\frac{\boldsymbol{n}(\boldsymbol{r})}{4\pi} \times \left(\int_K \frac{\boldsymbol{\gamma}(\boldsymbol{\xi},\, t) \times (\boldsymbol{r} - \boldsymbol{\xi})}{|\boldsymbol{r} - \boldsymbol{\xi}|^3} \times \boldsymbol{n}(\boldsymbol{r}) dS_\xi \right) - \frac{\boldsymbol{\gamma}(\boldsymbol{r},\, t) \times \boldsymbol{n}(\boldsymbol{r})}{2} = \boldsymbol{f}(\boldsymbol{r},\, t), \quad \boldsymbol{r} \in K, \quad (5)$$

where the right-hand side $\boldsymbol{f}(\boldsymbol{r},\, t)$ is known vector function, which depends on the vortex wake influence and the incident flow velocity:

$$\boldsymbol{f}(\boldsymbol{r},\, t) = -\boldsymbol{n}(\boldsymbol{r}) \times ((\boldsymbol{V}_\infty + \boldsymbol{V}_\Omega(\boldsymbol{r})) \times \boldsymbol{n}(\boldsymbol{r})).$$

Note, that the kernel of the equation (5) is unbounded when $|\boldsymbol{r} - \boldsymbol{\xi}| \to 0$, so in order to solve it numerically with rather high accuracy the following assumptions are introduced:

1. The body surface is discretized into N triangular panels K_i with areas A_i and unit normal vectors n_i, $i = 1, ..., N$.

2. The unknown vortex sheet intensity on the i-th panel is assumed to be constant vector $\boldsymbol{\gamma}_i$, $i = 1, ..., N$, which lies in the plane of the i-th panel, i. e., $\boldsymbol{\gamma}_i \cdot \boldsymbol{n}_i = 0$.

3. The integral equation (5) is satisfied on average over the panel, or, the same, in Galerkin sense: its residual is orthogonal to the basis function which is equal to the 1 on the j-th panel and equal to 0 on all other panels.

According to these assumptions the discrete analogue of (5) can be derived:

$$\frac{1}{4\pi A_i} \sum_{j=1}^{N} \int_{K_i} \left(\int_{K_j} \boldsymbol{n}_i \times \left(\frac{\boldsymbol{\gamma}_j \times (\boldsymbol{r} - \boldsymbol{\xi})}{|\boldsymbol{r} - \boldsymbol{\xi}|^3} \times \boldsymbol{n}_i \right) dS_\xi \right) dS_r - \frac{\boldsymbol{\gamma}_i \times \boldsymbol{n}_i}{2} = \frac{1}{A_i} \int_{K_i} \boldsymbol{f}(\boldsymbol{r},\, t) dS_r,$$

$$i = 1, \ldots, N. \quad (6)$$

To write down (6) in the form of a linear algebraic system we choose local orthonormal basis on every cell ($\boldsymbol{\tau}_i^{(1)}$, $\boldsymbol{\tau}_i^{(2)}$, $\boldsymbol{n}_i$), where tangent vectors $\boldsymbol{\tau}_i^{(1)}$, $\boldsymbol{\tau}_i^{(2)}$ can be chosen arbitrary (in the plane of the cell, orthogonal one to the other) and $\boldsymbol{\tau}_i^{(1)} \times \boldsymbol{\tau}_i^{(2)} = \boldsymbol{n}_i$, so

$$\boldsymbol{\gamma}_i = \gamma_i^{(1)}\boldsymbol{\tau}_i^{(1)} + \gamma_i^{(2)}\boldsymbol{\tau}_i^{(2)},$$

and we can project (6) for every i-th panel on directions $\boldsymbol{\tau}_i^{(1)}$ and $\boldsymbol{\tau}_i^{(2)}$ [12, 13].

Note, that the obtained algebraic system has infinite set of solutions; in order to select the unique solution the additional condition for the total vorticity (the integral from the vorticity over the body surface) should be satisfied:

$$\int_K \boldsymbol{\gamma}(\boldsymbol{r},\, t)dS_r = \boldsymbol{0},$$

which also should be written down in the discretized form.

The resulting algebraic system is overdetermined, it should be regularized similarly to [4] by introducing the regularization vector $\boldsymbol{R} = (R_1,\, R_2,\, R_3)^T$:

$$\frac{1}{4\pi A_i}\boldsymbol{\tau}_i^{(1)} \cdot \left(\sum_{j=1}^N \gamma_j^{(1)}\boldsymbol{\nu}_{ij}^{(1)} + \sum_{j=1}^N \gamma_j^{(2)}\boldsymbol{\nu}_{ij}^{(2)}\right) - \frac{\gamma_i^{(2)}}{2} + \boldsymbol{R}\cdot\boldsymbol{\tau}_i^{(2)} = \frac{b_i^{(1)}}{A_i},$$

$$\frac{1}{4\pi A_i}\boldsymbol{\tau}_i^{(2)} \cdot \left(\sum_{j=1}^N \gamma_j^{(1)}\boldsymbol{\nu}_{ij}^{(1)} + \sum_{j=1}^N \gamma_j^{(2)}\boldsymbol{\nu}_{ij}^{(2)}\right) + \frac{\gamma_i^{(1)}}{2} + \boldsymbol{R}\cdot\boldsymbol{\tau}_i^{(1)} = \frac{b_i^{(2)}}{A_i}, \qquad (7)$$

$$\sum_{j=1}^N A_j\left(\gamma_j^{(1)}\boldsymbol{\tau}_j^{(1)} + \gamma_j^{(2)}\boldsymbol{\tau}_j^{(2)}\right) = 0, \qquad i = 1,\,\ldots,\,N.$$

The semi-analytical numerical algorithm is developed [12, 13] for the integrals calculation in the coefficients

$$\boldsymbol{\nu}_{ij}^{(k)} = \int_{K_i}\left(\int_{K_j}\frac{\boldsymbol{\tau}_j^{(k)} \times (\boldsymbol{r} - \boldsymbol{\xi})}{|\boldsymbol{r} - \boldsymbol{\xi}|^3}dS_\xi\right)dS_r, \quad b_i^{(k)} = \int_{K_i}\boldsymbol{\tau}_i^{(k)} \cdot \boldsymbol{f}(\boldsymbol{r},\, t)dS_r.$$

Numerical experiments show that the developed algorithm permits to reconstruct surface vorticity distribution with rather high accuracy, even on coarse meshes and, that more important for practice, on non-uniform meshes with refinements. Velocity field, generated by such vorticity, is rather smooth near to the body surface.

In order to use this approach in the above described in section 3 algorithm of the vortex loops generation, it is necessary to reconstruct the double layer potential at the vertices of the surface mesh. The solution of linear system (7) gives us piecewise-constant vortex sheet intensity distribution over the panels. From the other side, vortex sheet intensity is surface gradient of the double layer potential density. It means, that the most convenient way to double layer potential density recovery is its approximation by a function, which is piecewise-linear at the panels. To do it, we consider the nodal values of the potential g_j, $j = 1,\,\ldots,\,M$ to be unknown; M is number if vertices of the surface mesh. Then

the potential density can be recovered by FEM-type interpolation using 1-st order shape functions. Let us note positions of al the vertices of the surface mesh as $\boldsymbol{\rho}_j$, $j = 1, \ldots, M$, the vertices of the i-th triangular panel have indices p_i^k, $k = 1, 2, 3$. The shape functions, defined over the i-th panel, coincides with barycentric coordinates on the triangle:

$$\phi_i^{(k)}(\boldsymbol{\rho}) = \frac{|(\boldsymbol{\rho}_{p_i^l} - \boldsymbol{\rho}) \times (\boldsymbol{\rho}_{p_i^m} - \boldsymbol{\rho})|}{|(\boldsymbol{\rho}_{p_i^l} - \boldsymbol{\rho}_{p_i^k}) \times (\boldsymbol{\rho}_{p_i^m} - \boldsymbol{\rho}_{p_i^k})|}, \quad \boldsymbol{\rho} \in K_i,$$

where $(k, l, m) = (1, 2, 3)$, or $(2, 3, 1)$ or $(3, 1, 2)$, then the double layer density over the i-th panel is linear function with respect to $\boldsymbol{\rho}$ and has the form

$$g(\boldsymbol{\rho}) = \sum_{k=1}^{3} g_{p_i^k} \phi_i^{(k)}(\boldsymbol{\rho}), \quad \boldsymbol{\rho} \in K_i.$$

The gradient of the approximate double layer on the every i-th panel, multiplied by normal unit vector $\boldsymbol{n}_i$ gives the constant vector, which physical sense is approximate value of vortex sheet intensity at the corresponding panel:

$$\boldsymbol{\gamma}_i^* = -\sum_{k=1}^{3} g_{p_i^k} (\operatorname{Grad} \phi_i^{(k)} \times \boldsymbol{n}_i), \quad \boldsymbol{\rho} \in K_i,$$

where the surface gradients of the shape functions $\operatorname{Grad} \phi_i^{(k)}$ are constant vectors.

The unknown values g_j can be found from the least-squares procedure:

$$\Psi = \sum_{i=1}^{N} |\boldsymbol{\gamma}_i - \boldsymbol{\gamma}_i^*|^2 \to \min.$$

Taking partial derivatives of Ψ with respect to g_j, $j = 1, \ldots, M$, and making them equal to zero, we obtain linear system of $M \times M$ size with symmetric matrix.

This system is singular (in practice, due to the truncation errors, it is ill-conditioned), that follows from the fact, that the value of potential density can be chosen arbitrary at some arbitrary specified point. We assume $g_M = 0$, that means that the last row and last column in least-squares matrix should be nullified, the diagonal coefficient can be chosen arbitrary (non-zero); the last coefficient in the right-hand side also should be nullified. The resulting regularized matrix is symmetric and positively defined.

5   VORTEX WAKE SIMULATION

The developed modification of vortex method is based on the closed vortex loops usage for numerical simulation of the vortex wake and its evolution. The vortex wake is considered to consist of K closed vortex loops of the same circulation Γ.

The loop with index k, $k = 1, ..., K$ is simulated by the polygonal vortex line (vortex filament) with N_k vertices. These vertices are considered as the Lagrangian markers $\boldsymbol{r}_{k,i}$, $i = 1, ..., N_k$, moving in the flow along the streamlines; their motion is described by ODE:

$$\frac{d\boldsymbol{r}_{k,i}}{dt} = \boldsymbol{V}(\boldsymbol{r}_{k,i}, t), \boldsymbol{r}_{k,i}(0) = \boldsymbol{r}_{k,i}^0, i = 1, ..., N_k, k = 1, ..., K. \tag{8}$$

We assume the loop legs between two neighboring vertices to be rectilinear line segments, which are described by vectors

$$\Delta \boldsymbol{r}_{k,i} = \boldsymbol{r}_{k,i+1} - \boldsymbol{r}_{k,i}, i = 1, ..., N_k, k = 1, ..., K.$$

They induce the velocities $\Gamma \boldsymbol{v}_{k,i}(\boldsymbol{r})$, which can be calculated analytically as vortex fragmentons influences, regularized by introducing of small smoothing radius ε and finally give contribution to the velocity field $\boldsymbol{V}_\Omega$, generated by vortex wake:

$$\boldsymbol{V}_\Omega(\boldsymbol{r}, t) = \Gamma \sum_{l=1}^{K} \sum_{m=1}^{N_k} \boldsymbol{v}_{l,m}(\boldsymbol{r}, t).$$

Numerical integration of system (8) is carried out by using explicit Euler method with constant step Δt. Initial conditions for markers positions in (8) are parameters of the loops at the time of their generation on the body surface.

Firstly, maximal and minimal values of the double layer intensity for all the panels vertices on the body surface $g_{\max} = \max\limits_{j=1,...,M} g_j$ and $g_{\min} = \min\limits_{j=1,...,M} g_j$ should be found. The panels are assumed to be triangular, as it was mentioned above, so it is easy to construct level lines of the potential density, which correspond to potential values, which differ from one to another on value Γ. These level lines determine the initial shape of the vortex loops. For the given value of the potential density there can be one or more closed level lines, which correspond to separate vortex loops. The number of level lines values is determined as the integer part of expression

$$N_q = [(M - m)/\Gamma] - 1. \tag{9}$$

Then the generated vortex loops become part of vortex wake. The vortex loops, generated on the surface, should be shifted from the surface in normal direction on small constant distance Δ. It should be noted, that the contribution of the vortex loop to the velocity field $\boldsymbol{V}_\Omega(\boldsymbol{r}, t)$ is not considered at the time step immediately after its generation, and for velocity field influence of the corresponding panels on the body surface (which give contribution to $\boldsymbol{V}_\gamma(\boldsymbol{r}, t)$) is taken into account.

When vortex elements move in the flow, some marker positions can intersect the body surface, mainly due to numerical errors in velocity field reconstruction and vorticity motion equations integration. In such cases, the loop legs, which intersect the body surface, is replaced with some other loop legs, which lay on the body surface and provide the shortest way. The Dijkstra's algorithm is used for such procedure [14].

At every time step several procedures for smoothing of loops geometry, loop segments length alignment and loops reconnection are used [15]. It is necessary to control the angle values between the neighboring line segments in vortex loops:

$$\psi_{k,i} = \arccos\left(\frac{\Delta \boldsymbol{r}_{k,i} \cdot \Delta \boldsymbol{r}_{k,i-1}}{|\Delta \boldsymbol{r}_{k,i}| \cdot |\Delta \boldsymbol{r}_{k,i-1}|}\right).$$

If for some vortex loop vertex $\psi_{k,i} < \varphi$, where φ is a given constant, then vertex position should be corrected.

After angle correction, when the vortex loops are smooth enough, it is necessary to "rediscretize" them in order to provide nearly the same length h for all the segments. In this procedure cubic spline interpolation is used in order to reconstruct smooth shape of the vortex filaments.

Vortex loops reconnection is carried out according to the following algorithm. For each marker $\boldsymbol{r}_{k,i}$ the nearest marker $\boldsymbol{r}_{l,j}$ is searched ($j = 1, ..., N_l$, $l = 1, ..., K$), for which the conditions are satisfied:

$$|\boldsymbol{r}_{l\,j} - \boldsymbol{r}_{k\,i}| < \mu, \quad \arccos\left(\frac{\boldsymbol{D}_{k,i} \cdot \boldsymbol{D}_{l,j}}{|\boldsymbol{D}_{k,i}| \cdot |\boldsymbol{D}_{l,j}|}\right) > \varphi, \tag{10}$$

where $\mu > 0$ is some given value, $\boldsymbol{D}_{l,j} = \boldsymbol{r}_{l,j+1} - \boldsymbol{r}_{l,j-1}$, $\boldsymbol{D}_{k,i} = \boldsymbol{r}_{k,i+1} - \boldsymbol{r}_{k,i-1}$.

From all the marker pairs, for which conditions (10) are satisfied, that pair is selected, for which $|\boldsymbol{r}_{l,j} - \boldsymbol{r}_{k,i}|$ has minimal value, and the reconnected is performed for the copesponding legs. In this procedure either two vortex loops are formed from one, or, vice verca, two loops are merged into one. Then for the newly formed vortex loop (or loops) the reconnection algorithm is repeated.

6   NUMERICAL RESULTS

Let us consider firstly the results of double layer potential density reconstruction according to the "direct" method (see Section 3) and to the "indirect" one (through vortex sheet intensity recovery intermediate step, see Section 4).

The results are shown in the Fig. 1 for the sphere discretized into 714 triangular panels of nearly the same size. The incident flow is directed vertically (upward). It is seen that the indirect approach leads to more accurate results: level lines are more smooth and very close to be horizontal, that corresponds to the considered problem.
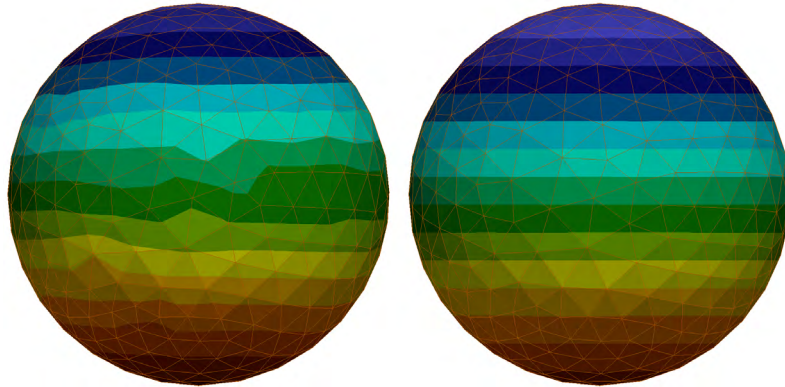
Figure 1: Level lines of the double layer potential density, obtained "directly" (left picture) and "indirectly" (right picture) on the uniform mesh

The "indirect" algorithm permits to obtain rather good results also on coarse and non-uniform meshes. In Fig. 2 the same sphere is split into 342 panels when the ratio of the largest panel area to the smallest one is close to 32. The quality of the level lines shape remains high for "indirect" method, in opposite to the "direct" one.
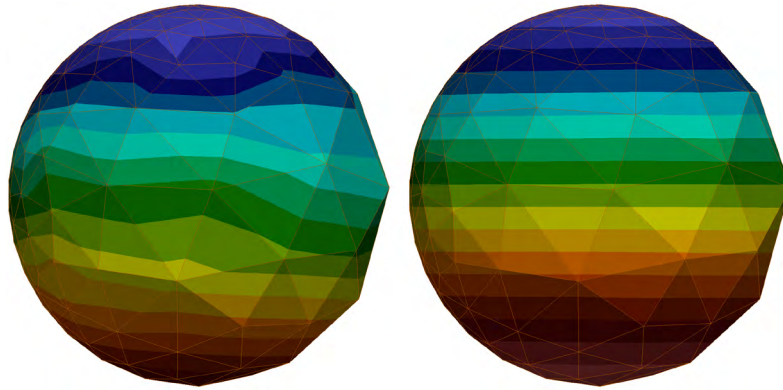
Figure 2: Level lines of the double layer potential density, obtained "directly" (left picture) and "indirectly" (right picture) on the coarse non-uniform mesh

The difference between two approaches is kept for the bodies of more complicated geometry. The example of the flow around doubly connected body: the model of sport weight is shown in Fig. 3; the incident flow is directed diagonally from low right to up left corner. The triangular mesh with local refinement was constructed in the Salome open-source software and consists of 636 panels.
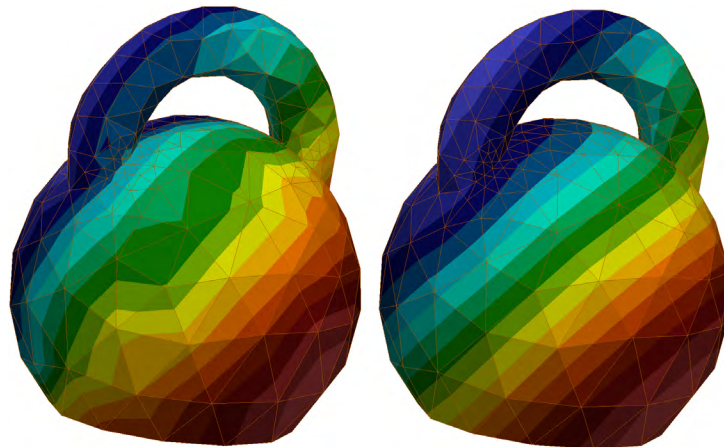
Figure 3: Level lines of the double layer potential density, obtained "directly" (left picture) and "indirectly" (right picture) for the body of complicated shape

For essentially non-uniform meshes, for example, obtained from the stl-file, which consist of large number of "bad" cells (elongated triangles with small angles) generated in some CAD software, the "direct" approach doesn't permit to obtain solution at all. At the same time the "indirect" approach makes it possible to reconstruct the solution with rather good quality (Fig. 4).

The example of unsteady flow simulation around the body of complicated shape (sport weight model) is shown in Fig. 5 for four different time steps. Number of loops during the simulation becomes rather small, however number of markers $P = \sum_{k=1}^{K} N_k$ grows, because the vortex loops length growth and their shape becomes complicate.
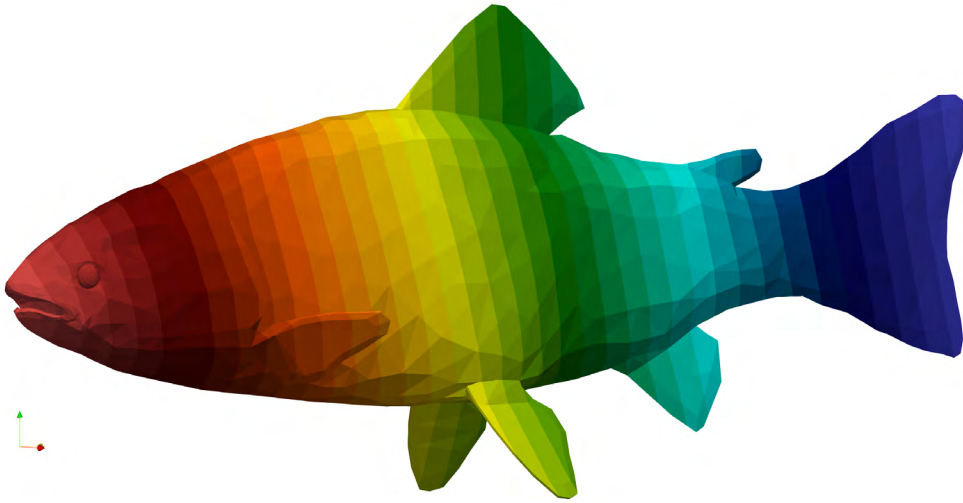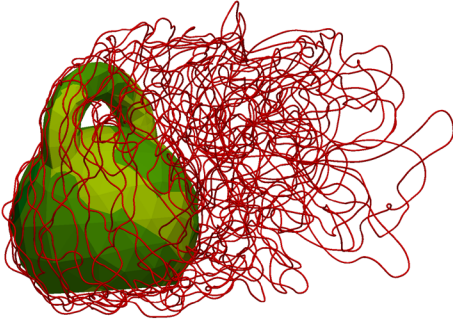
Figure 4: Level lines of the double layer potential density for the fish stl-model, obtained by using "indirect" method
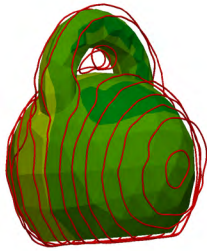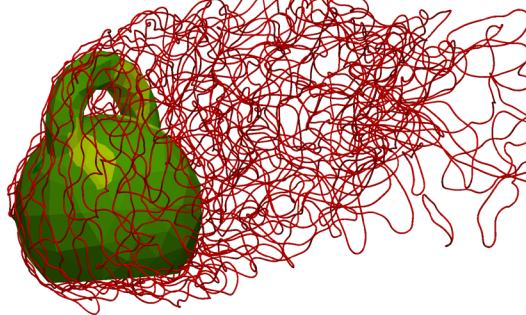

Time step no. 2.
Number of vortex loops $K = 17$
Number of markers $P = 2\ 077$
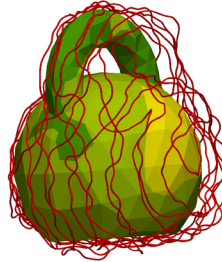
Time step no. 10.
Number of vortex loops $K = 8$
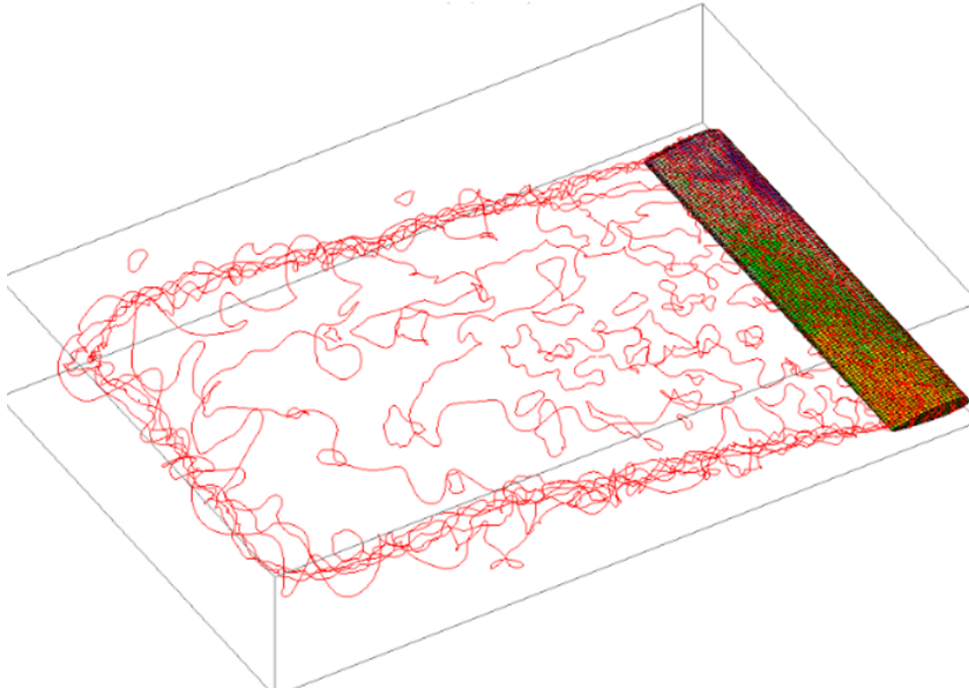Number of markers $P = 13\ 386$

Time step no. 100.
Number of vortex loops $K = 7$
Number of markers $P = 9\ 713$

Time step no. 150.
Number of vortex loops $K = 14$
Number of markers $P = 12\ 573$

Figure 5: Vortex wake behind the sport weight model. Incident flow is directed from left to right. Vortex loops are shown as red lines

The application of the developed technique for the flow simulation around the wind model of the finite span (with elongation 5), is shown in Fig. 6. High quality of the boundary condition satisfaction on the body surface, provides good self-organization of the vortex wake. Clear structure of the Prandtl's horseshoe vortex is seen. Note, that this result is obtained without any additional hypotheses about flow separation line position or any equal suggestions.

Figure 6: Vortex wake structure behind the wing model. Incident flow is directed from right to left. Time step no. 360, number of vortex loops $K = 109$, number of markers $P \approx 20\,000$.

7 CONCLUSION

The developed algorithm permits to improve significantly the quality of the double layer potential density reconstruction for the bodies with very complicated geometry and low-quality surface meshes. Its numerical complexity is higher than for the "direct" one due to solution of twice-larger linear system to recover vortex sheet intensity and the least-square problem. The combination of this approach with vortex wake modelling with vortex loops, makes it possible to simulte unsteady flows with higher resolution with acceptable numerical complexity. The developed approach can be useful for CFD applications and visual effects reproducing in computer graphics.

REFERENCES

[1] Cottet, G.-H. and Koumoutsakos, P. *Vortex Methods: Theory and Practice.* CUP, (2000).

[2] Lewis, R.I. *Vortex Element Methods for Fluid Dynamic Analysis of Engineering Systems.* CUP, (2005).

[3] Weissmann, S. and Pinkall, U. Filament-based smoke with vortex shedding and variational reconnection. *ACM Trans. Graph* (2010), **29(4)**:115.

[4] Lifanov, I.K., Poltavskii, L.N. and Vainikko, G.M. *Hypersingular Integral Equations and Their Applications.* CRC Press, (2003).

[5] Kamemoto, K. On Contribution of Advanced Vortex Element Methods Toward Virtual Reality of Unsteady Vortical Flows in the New Generation of CFD. *J. of the Brazilian Society of Mechanical Sciences and Engineering* (2004), **26(4)**:368–378.

[6] Alkemade, A.J.Q. *On Vortex Atoms and Vortons.* Ph.D. Thesis, Delft (1994).

[7] Kempka, S.N. et al, Accuracy considerations for implementing velocity boundary conditions in vorticity formulations. SANDIA Rep SAND96-0583 UC-700, 1996.

[8] Timofeev, V.N. Mathematical simulation of the subsonic flow around the lengthening bodies with the flow separation in the region of ground shear with the use of an equivalent body. *Journal of Physics: Conference. Series.* (2018) **1141**:012095.

[9] Saffman, P.G. *Vortex Dynamics.* CUP (1992).

[10] Shcheglov, G.A. and Dergachev, S.A. Hydrodynamic Loads Simulation for 3D Bluff Bodies by Using the Vortex Loops Based Modification of the Vortex Particle Method. *5th International Conference on Particle-Based Methods — Fundamentals and Applications* (2017), 725–731.

[11] Kuzmina, K.S., Marchevskii, I.K. and Moreva, V.S. Vortex Sheet Intensity Computation in Incompressible Flow Simulation Around an Airfoil by Using Vortex Methods. *Mathematical Models and Computer Simulations.* (2018). **10(3)**:276–287.

[12] Marchevsky, I.K. and Shcheglov, G.A. Efficient Semi-Analytical Integration of Vortex Sheet Influence in 3D Vortex Method. *5th International Conference on Particle-Based Methods — Fundamentals and Applications* (2017), 703–714.

[13] Marchevsky, I.K. and Shcheglov, G.A. Semi-analytical influence computation for vortex sheet with piecewise constant intensity distribution in 3D vortex methods. *6th Eur. Conf. on Comput. Mech. (ECCM 6), 7th Eur. Conf. on Comput. Fluid. Dyn. (ECFD 7)* (2018), 2410–2421.

[14] Dijkstra, E.W. A note on two problems in connexion with graphs. *Numerische Mathematik* (1959), **1**:269–271.

[15] Shcheglov, G.A. and Dergachev, S.A. Vortex Loops Based Method for Subsonic Aerodynamic Loads Calculation. *MATEC Web of Conferences* (2018) **221**:05004.